Mineralogy and geochemistry of platinum-group elements in the Aguablanca Ni-Cu deposit (SW Spain)

R. Piña[1], **F. Gervilla**[2], **L. Ortega**[1], and **R. Lunar**[1]

[1] Departamento de Cristalografía y Mineralogía, Facultad de Geología, Universidad Complutense de Madrid, Madrid, Spain
[2] Facultad de Ciencias, Instituto Andaluz de Ciencias de la Tierra, Universidad de Granada-CSIC, Granada, Spain

Summary

The Aguablanca Ni-Cu-(PGE) magmatic sulphide deposit is associated with a magmatic breccia located in the northern part of the Aguablanca gabbro (SW, Iberia). Three types of ores are present: semi-massive, disseminated, and chalcopyrite-rich veined ore. The principal ore minerals are pyrrhotite, pentlandite and chalcopyrite. A relatively abundant platinum-group mineral (PGM) assemblage is present and includes merenskyite, melonite, michenerite, moncheite and sperrylite. Moreover, concentrations of base and precious metals and micro-PIXE analyses were obtained for the three ore-types. The mineralogy and the mantle-normalised chalcophile element profiles strongly suggest that semi-massive ore represents *mss* crystallisation, whereas the disseminated ore represents an unfractionated sulphide liquid and the chalcopyrite-rich veined ore a Cu-rich sulphide liquid. Palladium-bearing minerals occur commonly enclosed within sulphides, indicating a magmatic origin rather than hydrothermal. The occurrences and the composition of these minerals suggest that Pd was initially dissolved in the sulphides and subsequently exsolved at low temperatures to form bismutotellurides. Negative Pt and Au anomalies in the mantle-normalised chalcophile element profiles, a lack of Cu-S correlation and textural observations (such as sperrylite losing its euhedral shape when in contact with altered minerals) suggest partial remobilisation of Pt, Au and Cu by postmagmatic hydrothermal fluids after the sulphide crystallisation.

Introduction

The Aguablanca Ni-Cu deposit (15.7Mt grading 0.66 wt.% Ni, 0.46 wt.% Cu and 0.47 g/t PGE) is an exceptional ore deposit from many points of view. It is located in one of the southernmost segments of the European Variscan chain, a collisional orogen mostly devoid of magmatic sulphide mineralisations. Its discovery in 1993 was the first report of this type of deposit in southwestern Spain (*Lunar* et al., 1997; *Ortega* et al., 2000) and promoted an intense exploration program in the region and the identification of new favorable targets. Mining operations started in 2004. Two features of Aguablanca are unusual for a Ni-sulphide deposit (*Tornos* et al., 2001; *Piña* et al., 2006): 1) It is related to the development of calc-alkaline magmatism in a collisional margin, rather than in a rift environment, more common for these deposits (*Barnes* and *Lightfoot*, 2005), and 2) it is hosted by a subvertical magmatic breccia which derived from an underlying concealed magmatic chamber. In this complex structural scenario, the distribution of ores and metals in the deposit was determined by a) the fractional crystallisation processes of the silicate melt and b) the timing of the sulphide liquid segregation relative to the emplacement of the breccia and its subsequent evolution. The post-magmatic circulation of hydrothermal fluids overprinted the sub-solidus re-equilibrated magmatic assemblages and partially modified the deposit (*Ortega* et al., 2004). These key factors are now well constrained (*Piña* et al., 2005, 2006, and this work) and allow a better understanding of the geochemical and mineralogical characteristics of the Aguablanca deposit.

The aim of this paper is to present a detailed study of the whole rock chemistry of the ore, the mineralogy of the platinum-group elements and the micro-PIXE analysis of the sulphides. These data are then discussed in order to explain the behaviour of the chalcophile elements and the origin of the PGM during the segregation and fractionation of the sulphide melt, the crystallisation of the sulphides and the late hydrothermal alteration processes.

Geological background

The Aguablanca deposit is located in the northern part of the Aguablanca intrusion. This intrusion crops out in the southern limb of the Olivenza-Monesterio antiform, a WNW-ESE trending, longitudinal, Variscan structure situated in the southern part of the Ossa-Morena Zone (OMZ) (Fig. 1) (*Riveiro* et al., 1990; *Sánchez-Carretero* et al., 1990; *Eguiluz* et al., 2000). The OMZ is one of the tectonic domains of the Iberian Massif which includes extensive outcrops of Pre-Mesozoic rocks in the Iberian Peninsula. A detailed review of the Iberian Massif is given by *Quesada* (1991) and references therein.

The Aguablanca intrusion shows a subcircular outcrop of 3 km^2 and comprises mostly massive gabbro merging to the south with diorite and to its northern zone with gabbronorite. It intrudes Early Cambrian volcanic, volcanoclastic and carbonate rocks (Bodonal-Cala Complex) which overlie Late Precambrian metasedimentary rocks mainly composed of graywackes and pyrite-rich black slates (Serie Negra Formation) (*Eguiluz* et al., 2000) (Fig. 1). Preliminary analytical data show that the black slates of the Serie Negra are rich in S (up to 5238 ppm) and show S/Se ratios

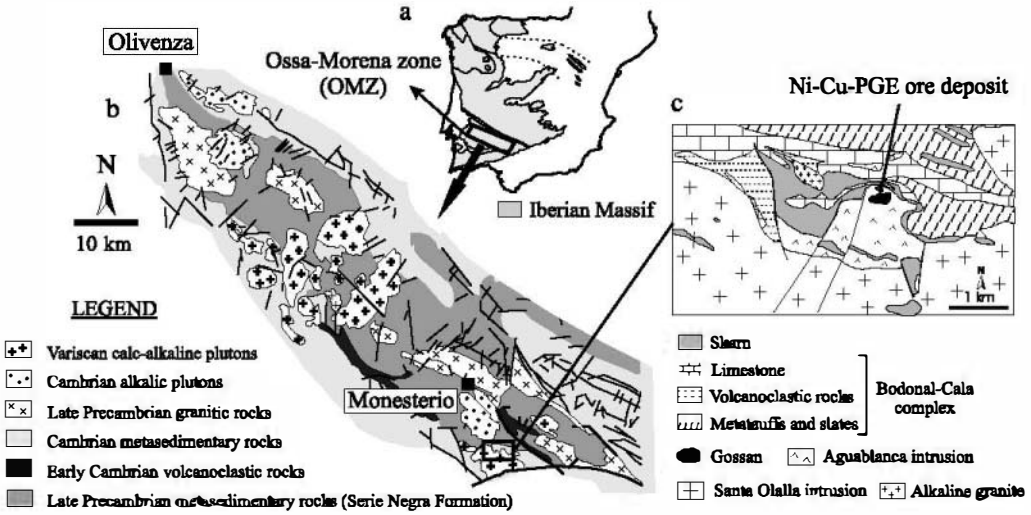

Fig. 1. **a** Location of the Ossa-Morena zone in the Iberian Massif. **b** Simplified regional geological map of the Olivenza-Monesterio antiform. **c** Schematic geological map of the Aguablanca area showing the location of the Ni-Cu-PGE ore (Lat. 37°57′N; Long. 6°11′W)

ranging from 184 to 3300 (1436 on average). Country rocks were metamorphosed during the Hercynian regional metamorphism which reached lower greenschist-facies conditions (*Quesada* and *Munha*, 1990). Along the contact with the intrusion, carbonate rocks were metamorphosed to skarn. The larger Santa Olalla intrusion occurs to the south of the Aguablanca intrusion (Fig. 1). It is formed by granodiorite and monzogranite in the core and tonalite and quartzdiorite at the rim (*Tornos* et al., 2001). Zircon U-Pb ages give an age of crystallisation for the Aguablanca intrusion of 338.6 ± 0.8 My (*Romeo* et al., 2004) which is in agreement with Ar^{40}-Ar^{39} ages on phlogopite of 338 ± 3 My (*Tornos* et al., 2004). Zircon U-Pb data for the Santa Olalla intrusion give an age of crystallisation of 341 ± 3 My (*Romeo* et al., 2004). These ages indicate that both the Aguablanca and Santa Olalla intrusion intruded during the Hercynian orogeny, which in the OMZ involved a main magmatic event characterised by the emplacement of calc-alkaline igneous rocks in response to the formation of an Andean-type magmatic arc (*Quesada* et al., 1994).

Analytical methods

Platinum-group minerals were identified and analysed on carbon coated sections under back-scattered mode with a JEOL Superprobe JXA-8900 M electron microprobe at the Electron Microscopy Centre "Luis Bru" of the University Complutense of Madrid, Spain. Quantitative analyses of the PGM were determined by WDS X-ray emission spectrometry. The accelerating voltage was 20 kV, the beam current 30 nA and the counting periods ranged from 20 to 60 s. Pure metals and synthetic alloys were used as standards. The X-ray lines analysed were As$L\alpha$, Fe$K\beta$, S$K\alpha$, Ni$K\alpha$, Bi$M\alpha$, Te$L\alpha$, Os$L\alpha$, Ir$L\alpha$, Ru$L\alpha$, Rh$L\alpha$, Pt$L\alpha$ and Pd$L\beta$. The software applies the peak-overlap correction method.

The micro-PIXE analyses of pyrrhotite, pentlandite, chalcopyrite and pyrite were carried out at the Scanning Proton Microprobe facility, University of Guelph, Department of Physics, Ontario, Canada. The analytical conditions were: beam current, between 3.75 and 8 nA at 3 MeV; beam size, 3 μm×6 μm; and counting times, between 120 and 190 s. The data were calculated using the GUPIX program (*Maxwell* et al., 1989). Detection limits are different for each element and depend on the mineral analysed. They range between 6–15 ppm for Pd, 6–13 ppm for Rh, 4–11ppm for Ru, 5–15ppm for Se, 25–800ppm for Ni, 17–1000ppm for Cu, 11–400ppm for Zn, 5–14 ppm for Ag and 6–30ppm for As.

Twenty-seven representative mineralised rock samples from the different ore-types were analysed for PGE, Au S, Se, Te, Bi, Ni, Cu and Co. PGE and Au were analysed by ICP-MS (nickel sulphide digest), S, Ni, Cu and Co by ICP-OES (multi-acid digest) and Bi, Se and Te by ICP-MS (multi-acid digest) in Genalysis Laboratory Services Pty. Ltd., Maddington (Western Australia). Detection limits were 10 ppm for S, 2 ppm for Se, 0.01 ppm for Te and Bi and 1 ppm for Ni, Cu and Co. For the noble metals, detection limits were 5 ppb for Au, 2 ppb for Ir, Os, Ru, Pd and Pt and 1 ppb for Rh.

The Ni-Cu-PGE ore deposit

Structure of the ore deposit and host rocks

The sulphide ore occurs within a subvertical (dipping 70–80° N) funnel-like breccia body (Fig. 2) composed of rocks containing semi-massive and disseminated sulphides which host variable amounts of mafic-ultramafic fragments. The mineralised breccia body is roughly 600 m long, 350–400 m wide and more than 700 m deep. The orebody exhibits a concentric structure made up of: 1) a core formed by

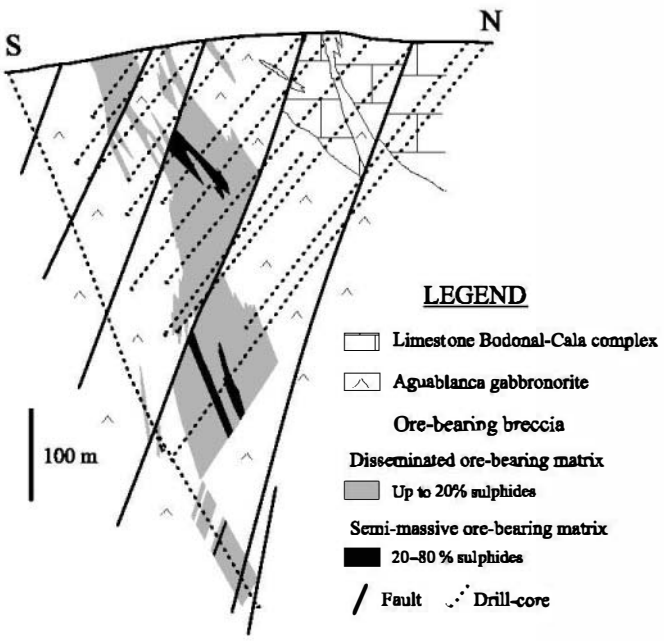

Fig. 2. North-south-oriented schematic cross section showing the ore-bearing breccia, based on drill core information. Mafic-ultramafic fragments are dispersed throughout the mineralised matrix

a ground mass of Ni-Cu-Fe sulphides with cumulus orthopyroxene, clinopyroxene, plagioclase and/or minor olivine which includes abundant randomly distributed, barren or very slightly mineralised fragments of mafic-ultramafic rocks (semi-massive ore); and 2) a gabbronorite envelope containing disseminated sulphides and minor mafic-ultramafic fragments (disseminated ore) (Fig. 2). The semi-massive ore-bearing rocks resemble those described as leopardite at the Voisey's Bay ore deposit (*Evans-Lamswood* et al., 2000). The disseminated ore-bearing gabbronorites are predominantly hornblende-rich gabbronorite with minor norite, gabbro and gabbrodiorite, and grade outwards to free-sulphide rocks. Late subvertical, NE-oriented faults commonly truncate and displace the ore body.

The mafic-ultramafic fragments are centimetric size (up to 9 cm across), and have subangular to rounded shapes and sharp contacts with the matrix. They consist of different rock-types with typical cumulate textures: peridotite (including dunite, werhlite and harzburgite), pyroxenite (both ortho- and clinopyroxenite), gabbro (gabbro *s.s.*, gabbronorite, norite and hornblende gabbro) and anorthosite (*Piña* et al., 2004, 2006). The fragments are interpreted to belong to a deep differentiated mafic-ultramafic complex brecciated during the shallow, tectonic intrusion of the sulphide and silicate magma matrix (*Tornos* et al., 2001; *Piña* et al., 2004, 2006).

All these rocks are variably altered to two postmagmatic, low-temperature mineral assemblages: an early one with actinolite $\pm$ chlorite $\pm$ epidote $\pm$ albite $\pm$ serpentine, followed by talc $\pm$ chlorite $\pm$ carbonates.

Ore mineralogy

The ore mineral assemblage is mainly composed of pyrrhotite, pentlandite, chalcopyrite and pyrite, with minor amounts of magnetite, ilmenite, platinum-group minerals (PGM), native gold, galena, tsumoite, tellurobismuthite, bismuthinite, members of the cobaltite-gersdorffite solid solution series, hessite, volinskyite, marcasite and violarite. Textural and mineralogical features of the ore have been described in detail by *Ortega* et al. (2004). Modal variations and the relative abundance of sulphides along the ore-body allow the identification of three main ore-types: semi-massive, disseminated and chalcopyrite veinlets:

(i) The semi-massive ore contains euhedral-subhedral grains of pyroxene, plagioclase and/or olivine, as well as mafic-ultramafic fragments. The modal sulphide content ranges between 20 and 85% (most of the samples have above 40% sulphides). Pyrrhotite is by far the predominant mineral (34–77% of the bulk ore minerals). It forms large anhedral twinned crystals, is commonly surrounded by polycrystalline, chain-like aggregates of pentlandite (11–34 mod.%) and shows exsolution flames of pentlandite along grain boundaries of pyrrhotite and fractures. Chalcopyrite (commonly below 11 mod.%) occurs as anhedral grains or as a polycrystalline intergrowths with pyrrhotite. Pentlandite:chalcopyrite ratio varies between 0.63 and 67.73. Isolated subhedral crystals of Cr-magnetite and ilmenite (up to 2%) often occur within pyrrhotite and interstitial to sulphides.

(ii) The disseminated ore is formed by inequigranular aggregates of polymineralic sulphides comprising less than 20% of the rock, which occur interstitially to

the silicate framework. Variable amounts of pyrrhotite (21–68 mod.%) form irregular grains, frequently rimmed by grains of pentlandite (3–18 mod.%) and chalcopyrite (12–58 mod.%). Chalcopyrite is commonly more abundant than pentlandite with pentlandite:chalcopyrite ratios below 1.0.

(iii) The chalcopyrite veinlets are cross-cutting the disseminated and semi-massive ores as well as the mafic-ultramafic fragments of the breccia. They are very small (<10 cm wide) and are mainly made up of massive chalcopyrite with minor amounts of irregular grains of pyrrhotite and pentlandite. Some subhedral grains of a Ag-Fe-Ni sulphide (likely argentopentlandite) are also included in chalcopyrite.

The sulphide assemblage described above is variably overprinted by hydrothermal pyrite (up to 16 mod.%), mostly in areas with strong microfracturing and intense retrograde alteration. Textural features, cross-cutting relationships and Ni and Co contents allowed to identify three main episodes of pyrite precipitation (Py_1, Py_2 + minor chalcopyrite, and Py_3) in which pyrite mostly replaces pyrrhotite (*Ortega* et al., 2004). The precipitation of Py_2 is coeval with the development of the actinolite ± chlorite ± epidote ± albite ± serpentine assemblage in the host silicate rocks, whereas Py_3 formed with the late talc ± chlorite ± carbonates assemblage. During the Py_2 episode, chalcopyrite locally occurs along cleavage planes of actinolite and chlorite.

Whole-rock chemistry of the ore

Sulphur concentrations are highly variable throughout the Aguablanca ores. In the semi-massive ores, S contents (12.7–30.4 wt.%) are markedly higher than those of the disseminated ores (2.3–8 wt.%) (Table 1) as expected from their higher sulphide contents. Sulphur and Se (7–74 ppm) are well correlated, with a correlation coefficient (ρ) of 0.97 (Table 2), indicating that the bulk of Se is in sulphide phases. S/Se ratio varies from 2613 to 4710; these values are within the empirical range of mantle-derived sulphides (*Naldrett*, 1981). In semi-massive ores, Ni (2.6–6.4 wt.%) commonly exceeds Cu (0.2–3.7 wt.%) with Ni/Cu ratios above 1 (average 7.3). This trend is reversed in the disseminated ores, where Cu contents (0.5–4 wt.%) exceed those of Ni (0.4–1.2 wt.%), with Ni/Cu ratios varying from 0.28 to 1.29 (average 0.85). These data are consistent with the higher chalcopyrite modal contents observed in the disseminated ores with respect to those in the semi-massive ores. As expected, Cu content in the chalcopyrite veinlets is high (up to 10.62 wt.%), with Ni remaining below 1 wt.%. Nickel and S are positively correlated (Fig. 3a), indicating that Ni occurs primarily in the sulphide phase. In contrast, Cu shows no correlation with S (Fig. 3b). Cobalt ranges from 96 to 2480 ppm, exhibiting a good positive correlation with S and Ni ($\rho = 0.90$ and 0.85, respectively) (Table 2).

Highly variable Au amounts are characteristics of the Aguablanca ore (from 15 to 911 ppb). Disseminated ores show higher Au contents than the semi-massive ones (Table 1). In the chalcopyrite veinlets, Au abundance ranges from 106 to 833 ppb. There is no correlation of Au with S or PGE (Table 2), but there is a relatively good correlation between Au and Cu ($\rho = 0.52$) (Fig. 3c).

Table 1. *Compositional data of mineralised samples, Aguablanca ore deposit*

Sample	S	Se	Te	Bi	Ni	Cu	Co	Au	Os	Ir	Ru	Rh	Pt	Pd	Total PGE	Ni/Cu	(Pd + Pt)/ (IPGE + Rh)	Pd/Ir_{MN}	Cu/Ni_{MN}	S/Se	Te/ (Pt + Pd)
Leopardite-textured semi-massive ore																					
Leopardite-6	20.26	57	3.4	2.60	4.63	3.19	1534	403	32	98	56	88	1581	1438	3293	1.45	11.02	12.04	45.01	3554	1.13
AGU-55-136	25.15	74	4.9	1.43	3.7	3.67	2480	738	55	154	110	157	1337	1438	3251	1.01	5.83	7.66	64.80	3399	1.77
Leopardite-2	20.12	64	3.7	2.50	5.85	0.62	1861	107	34	96	68	113	1187	1771	3269	9.44	9.51	15.14	6.92	3144	1.25
6554-235	27.74	61	1.5	1.89	5.57	0.53	1539	24	93	232	143	224	200	482	1374	10.51	0.99	1.70	6.22	4547	2.20
6580-279	30.01	67	1.4	2.97	6.24	0.93	1740	15	91	211	130	227	446	621	1726	6.71	1.62	2.41	9.74	4479	1.31
6715-415	26.28	64	2.4	10.64	6.3	0.49	1225	49	21	57	26	98	84	907	1193	12.86	4.91	13.06	5.08	4106	2.42
6580-281	30.42	65	1.1	3.77	5.7	1.83	1790	56	75	219	121	263	467	676	1821	3.11	1.69	2.53	20.98	4680	0.96
6715-416	26.24	57	2.1	11.17	6.41	0.22	1101	20	25	61	31	93	30	1193	1433	29.14	5.82	16.05	2.24	4604	1.72
6730-198	14.68	39	5.3	4.92	3.46	0.24	941	93	16	39	24	49	823	891	1842	14.42	13.39	18.75	4.53	3763	3.09
Fragments-bearing semi-massive ore																					
Breccia-4	16.32	49	3	4.56	3.93	0.95	1035	170	20	63	38	61	952	1244	2378	4.14	12.07	16.20	15.79	3331	1.37
Breccia-1	12.74	36	1.5	1.29	3.09	0.73	981	21	19	56	42	73	681	823	1694	4.23	7.92	12.06	15.43	3539	1.00
6629-39	15.24	36	2	4.57	3.44	0.82	723	39	13	35	25	41	2244	768	3126	4.20	26.42	18.00	15.57	4233	0.66
6758-544	13.86	33	1.2	8.04	2.59	2.51	722	84	13	35	23	62	603	711	1447	1.03	9.88	16.67	63.32	4200	0.91
Breccia-10	16.49	36	1.5	1.51	2.73	2.06	849	335	15	45	31	49	576	699	1415	1.33	9.11	12.75	49.30	4581	1.18
Breccia-11	21.54	47	1.8	1.92	4.21	0.71	1236	63	18	56	37	64	352	793	1320	5.93	6.54	11.62	11.02	4583	1.57
Disseminated ore																					
6580-108	3.92	15	1.9	0.84	0.81	1.06	250	127	10	27	19	30	312	279	677	0.76	6.87	8.48	85.50	2613	3.21
6749-390	3.17	12	1.8	5.49	0.41	1.48	138	264	b.d.	b.d.	6	4	346	216	572	0.28	56.20		235.84	2642	3.20
6749-376	8.07	18	0.7	3.01	1.07	1.2	634	229	9	39	18	56	78	234	434	0.89	2.56	4.92	73.27	4483	2.24
6758-548	3.56	12	1.6	4.18	0.43	1.13	181	167	b.d.	b.d.	4	4	276	128	412	0.38	50.50		171.69	2970	3.96
6554-246	4.71	10	0.7	1.6	0.72	0.56	276	35	4	15	12	17	88	155	291	1.29	5.06	8.48	50.81	4710	2.88
AGU-5-29	3.76	14	1.9	5.89	0.8	0.85	212	341	b.d.	2	8	5	469	371	855	0.94	56.00	152.21	69.42	2686	2.26
6554-169	2.37	7	0.9	1.45	0.52	0.46	183	48	b.d.	6	5	8	147	132	298	1.13	14.68	18.05	57.79	3390	3.23
6730-212	4.61	13	2.4	3.13	0.87	1.11	271	301	b.d.	5	9	14	458	404	890	0.78	30.79	66.30	83.36	3545	2.78
6715-452	5.77	18	1.4	4.64	1.23	0.99	294	182	b.d.	3	5	6	185	386	585	1.24	40.79	105.57	52.59	3204	2.45
6715-455	6.07	14	1	2.7	0.36	4.03	96	911	b.d.	4	5	4	440	102	555	0.09	41.69	20.92	731.37	4334	1.85
Chalcopyrite veinlets																					
6479-44.2	4.7	12	0.8	2.33	0.99	1.62	276	106	5	15	10	21	45	371	467	0.61	8.16	20.29	106.91	3917	1.92
6479-45.6	7.07	19	1.3	3.26	0.97	4.76	284	833	3	8	8	12	737	618	1386	0.20	43.71	63.38	320.60	3721	0.96
6554-221*	16.9				0.79	10.6		262	13	25	17	28	150	2513	2746	0.07	32.08	82.17	874.56		

* Data obtained from *Ortega* et al. (2004). Values of S, Ni and Cu are in wt.%; Se, Te, Bi and Co in ppm; Au and PGE in ppb; *b.d.* below detection. Ratios $(Cu/Ni)_{MN}$ and $(Pd/Ir)_{MN}$ were calculated to a 100% sulphide fraction following the method of *Naldrett* (1981) and then normalised to mantle values from *McDonough* and *Sun* (1995)

Table 2. *Correlation coefficients between the analysed elements*

	Os	Ir	Ru	Rh	Pt	Pd	S	Cu	Ni	Co	Te	Bi	Au	Ag	Se
Os	1	0.99	0.98	0.97	0.11	0.03	0.79	−0.14	0.67	0.74	0.11	−0.08	−0.13	−0.24	0.74
Ir		1	0.99	0.98	0.13	0.23	0.83	−0.10	0.74	0.83	0.17	−0.12	−0.19	−0.29	0.81
Ru			1	0.96	0.21	0.27	0.81	−0.07	0.73	0.86	0.22	−0.20	−0.15	−0.32	0.81
Rh				1	0.11	0.26	0.87	−0.12	0.80	0.85	0.15	−0.02	−0.24	−0.33	0.84
Pt					1	0.36	0.21	0.03	0.26	0.38	0.54	−0.15	0.21	0.05	0.35
Pd						1	0.55	0.54	0.45	0.77	0.71	0.17	0.02	−0.19	0.79
S							1	0.01	0.93	0.90	0.33	0.22	−0.22	−0.29	0.97
Cu								1	−0.28	0.02	0.00	−0.20	0.52	0.72	−0.03
Ni									1	0.85	0.37	0.31	−0.36	−0.34	0.95
Co										1	0.52	−0.03	−0.10	−0.38	0.96
Te											1	0.08	0.14	−0.17	0.50
Bi												1	−0.20	0.15	0.18
Au													1	0.71	−0.15
Ag														1	−0.29
Se															1

Bulk PGE concentrations range from 291 to 3293 ppb and are well correlated with S abundances (Fig. 3d). A group of semi-massive samples showing high S contents but low bulk PGE concentration are characterised by being rich in secondary pyrite and exhibiting Pt negative anomalies in the mantle-normalised patterns as showed later. The main geochemical feature of PGE is the predominance of Pt and Pd over IPGE (Os, Ir, Ru) and Rh in all the analysed samples. (Pt + Pd)/(IPGE + Rh) ratios range from 0.99 to 56.20 with 80% of the values above 5. Disseminated ores tend to have higher (Pt + Pd)/(IPGE + Rh) ratios than semi-massive ores (Table 1). IPGE and Rh show strong correlation each them (>0.96), but no correlation with Pt (<0.21) or Pd (<0.27) (Table 2). Osmium, Ir, Ru and Rh contents exhibit strong positive correlations with S (>0.79) (Table 2). Palladium correlates relatively well with S ($\rho = 0.55$) (Fig. 3e) and Pt is poorly correlated with S ($\rho = 0.21$) (Fig. 3f). It is worthy to note that the group of samples which has high S contents and deviates from the main correlation trend contains abundant secondary pyrite replacing pyrrhotite. Palladium and Pt are better positively correlated with Te ($\rho = 0.71$ and 0.54, respectively) (Fig. 3g, h).

The mantle-normalised, PGE, Ni, Cu and Au patterns of the different ore-types are broadly similar, with overall positive slopes (Fig. 4). Gold and Pt exhibit a somewhat erratic distribution with significant variations in their abundances within individual ore-types. In some semi-massive ore samples, the patterns show pronounced negative Au and Pt anomalies which are also present in disseminated and chalcopyrite veined ores. The semi-massive samples with negative Pt anomalies are those with high S and secondary pyrite abundances and relatively low bulk PGE contents in the Fig. 3d. Figure 4 shows significant differences between the different ore-types: semi-massive ores are slightly richer in Ni, and notably richer in IPGE and Rh than disseminated ores, and show lower mantle-normalised Pd/Ir and Cu/Ni ratios (9.5 and 19.9 vs. 22.7 and 119.3, respectively). The average pattern of the chalcopyrite veined ores shows an even steeper positive slope, with

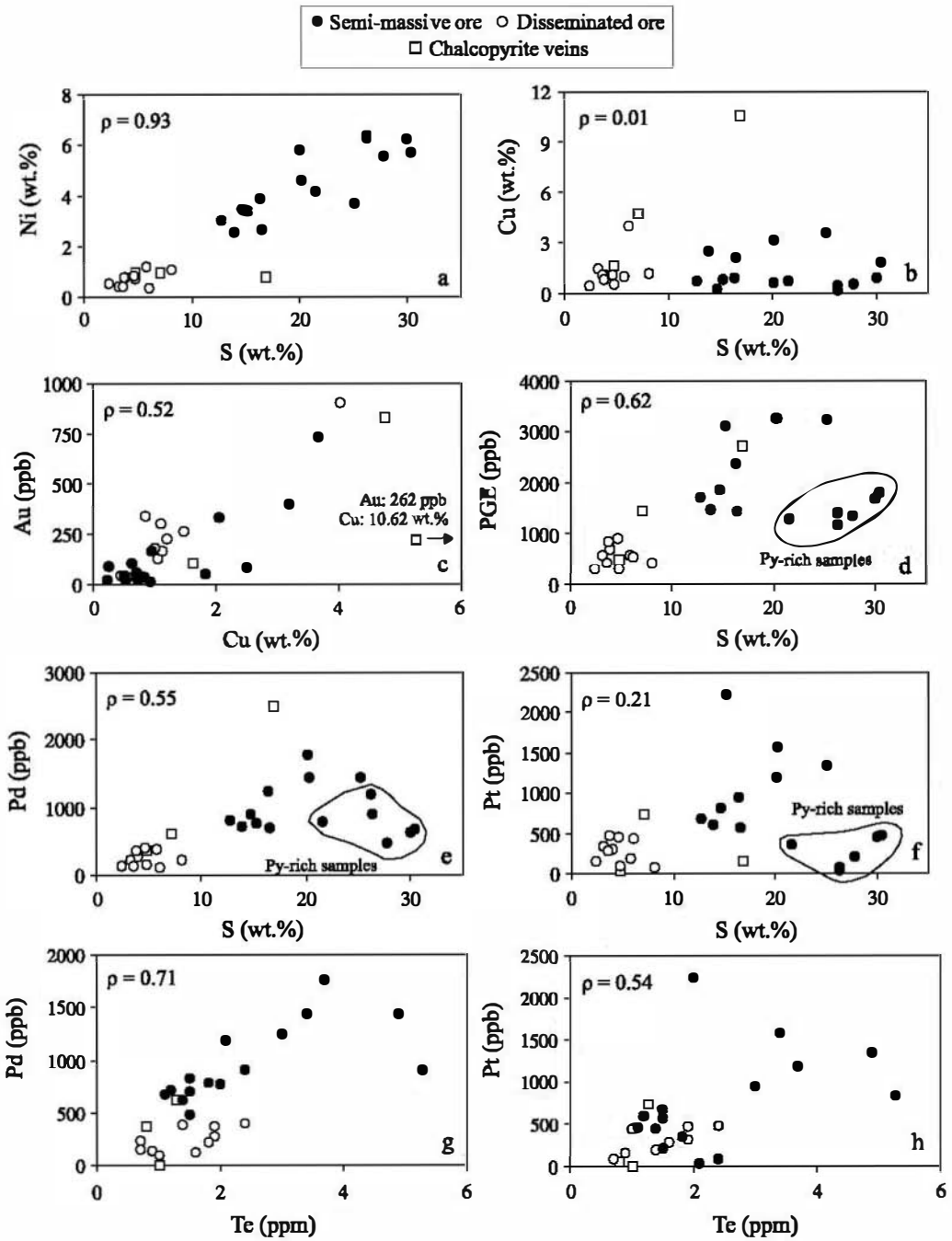

Fig. 3. Variation diagrams showing the correlations between different elements for samples from the ore-bearing breccia: **a** Ni vs. S; **b** Cu vs. S; **c** Au vs. Cu; **d** total PGE vs. S; **e** Pd vs. S; **f** Pt vs. S; **g** Pd vs. Te; **h** Pt vs. Te

mantle-normalised Pd/Ir and Cu/Ni ratios averaging 48.3 and 296, respectively. Figure 5 shows that: 1) most of the samples fall into the field of the layered intrusions, and 2) there is a gradual decrease in the Ni/Pd ratio with the increase

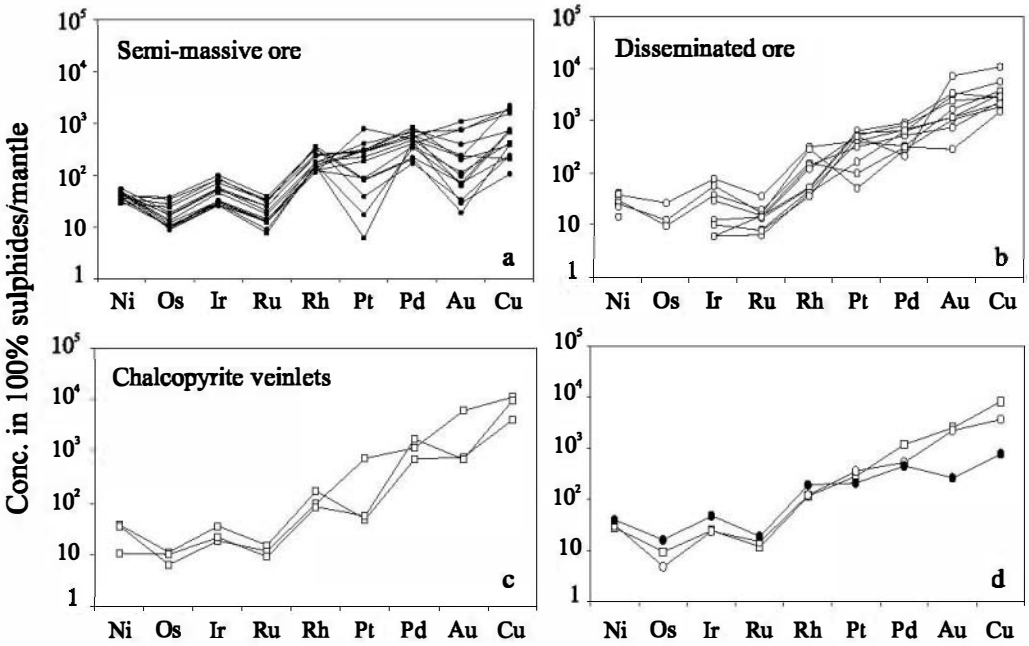

Fig. 4. Mantle-normalised metal patterns of the samples of the three ore-types from the ore-bearing breccia (**a**–**c**). **d** Mantle-normalised metal patterns for the average values. Normalisation factors are from *McDonough* and *Sun* (1995)

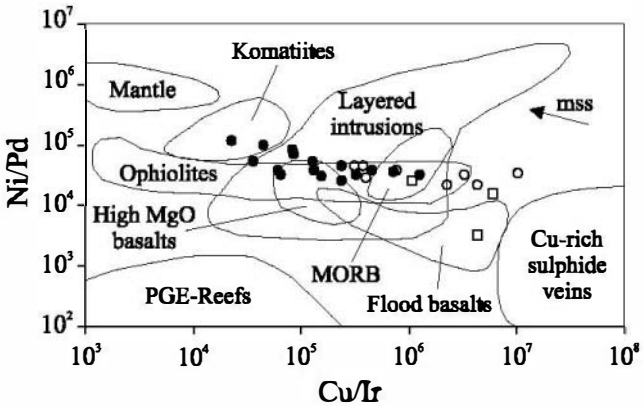

Fig. 5. Ni/Pd vs Cu/Ir ratios of the samples from the Aguablanca deposit compared with selected compositional fields after *Barnes* et al. (1988). Symbols as for Figs. 3 and 4

of the Cu/Ir ratio from the semi-massive to the disseminated ore and the chalcopyrite veined ores.

Mineralogy of the platinum-group elements

A total of 301 PGM grains were found in 45 polished sections representatives of the three ore-types. PGM are present in all ore-types, although they are substantially more abundant in the semi-massive (70.8% of the whole) and the chalcopyrite veined (21.2%) ores relative to the disseminated ore (uniquely 8.0% of the identified grains). Most PGM are spatially associated with base-metal sulphides. They occur included in sulphides (76%), along sulphide-silicate (11%) and

sulphide–sulphide (6%) grain boundaries, and only few of them are included in silicates (7%). More than 90% of the PGM grains are (Pd, Ni, Pt)-bismuthotellurides with the rest being sperrylite ($PtAs_2$), and phases containing Os-Ir-As-S, Ir-As-S and Ir-Pt-As (no quantitative analyses of these phases were obtained because of their very small grain sizes). (Pd, Ni, Pt)-bismuthotellurides consist, in a decreasing order of abundance, of merenskyite ($PdTe_2$), palladian melonite ($NiTe_2$), michenerite (PdBiTe) and moncheite ($PtTe_2$). Most PGM occur as single grains, although composite grains have occasionally been found. Some grains of the cobaltite-gersdorfitte solid solution series contain minor amounts of different PGE.

Merenskyite, Pd (-Ni, Pt)Te_2

Merenskyite represents 53% of the total PGM. In the disseminated and semi-massive ores, it forms small (<5–25 μm, but commonly less than 12 μm), rounded to subrounded grains hosted by pyrrhotite (Fig. 6a) and, more rarely, by pentlandite and chalcopyrite. It also occurs attached to the grain boundaries of sulphides (Fig. 6b). One unique grain has been observed in pyrite replacing pyrrhotite in semi-massive ores (Fig. 6c). Abundant grains of merenskyite, generally less than 10 μm across, were found in the chalcopyrite veinlets. These grains invariably occur within chalcopyrite (Fig. 6d) and along chalcopyrite-silicate grain boundaries.

The analyses of the larger grains reveal a wide compositional range (Table 3; Fig. 7a) in agreement with the solid-solution series existing between merenskyite and melonite (*Cabri*, 2002) and between merenskyite and moncheite (*Daltry* and *Wilson*, 1997; *Cabri*, 2002). Merenkyite shows a wide substitution of Pd by Ni (from 0.4 to 6.5 wt.%) and Pt (<17 wt.%). The grains found in the chalcopyrite veinlets do not contain Pt. There is an ubiquitous substitution of Te for Bi, ranging from 4.5 to 29 wt.%, in agreement with the compositions reported in the literature (*Harney* and *Merkle*, 1990; *Gervilla* and *Kojonen*, 2002; *Cabri*, 2002).

Palladian melonite, Ni (-Pd, Pt)Te_2

Palladian melonite only occurs in the semi-massive ores but represents 19% of the total PGM. The grain size rarely exceeds 10 μm, although some few crystals can be larger (up to 12 μm×25 μm). It forms rounded or elongated grains included in pentlandite (Fig. 6e) and, rarely, in pyrrhotite, or occurs attached to pentlandite-silicate interfaces (Fig. 6f). Palladian melonite occasionally occurs in composite grains with tellurobismuthite or michenerite.

Electron-microprobe analyses reveal a wide substitution of Ni by Pd (from 3.46 to 12.30 wt.% Pd) (Fig. 7a) and of Te by Bi (from 4.43 to 18.67 wt.% Bi) (Table 3). Melonite also contains variable proportions of Pt (<7.6 wt.%), although two Pd-rich grains also exhibit high Pt contents (12.58 and 16.75 wt.% Pt) (Fig. 7a).

Michenerite, PdBiTe

The modal proportion of michenerite (17%) is similar to that of melonite, although it occurs both in the semi-massive and in the disseminated ores, but not in chalcopyrite veinlets. Its shape and size (normally less than 15 μm) vary considerably,

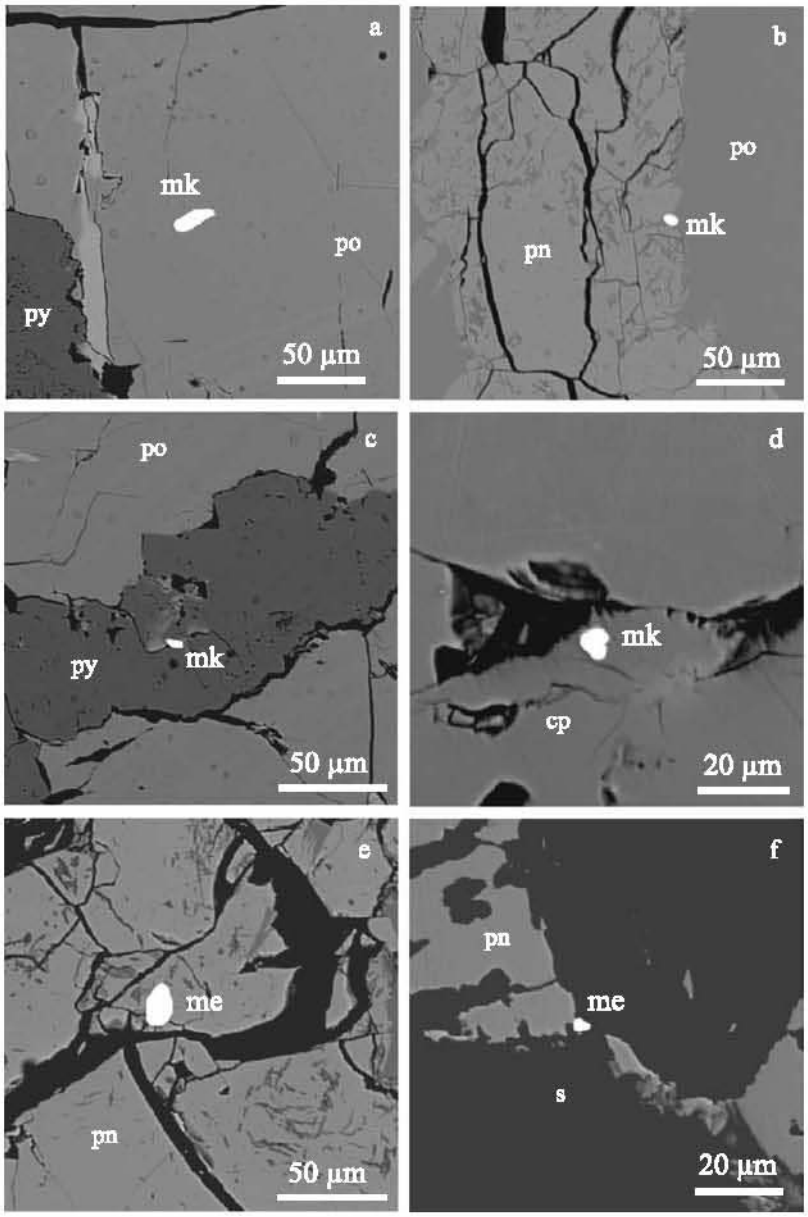

Fig. 6. Representative back-scattered electron microprobe images of the PGM. **a** Elongated merenskyite (*mk*) within pyrrhotite (*po*). **b** Subrounded merenskyite (*mk*) at the interface pentlandite (*pn*)-pyrrothite (*po*). **c** Merenskyite (*mk*) hosted in pyrite (*py*) replacing pyrrhotite (*po*). **d** Subrounded merenskyite (*mk*) within chalcopyrite (*cp*). **e** Rounded melonite (*me*) within pentlandite (*pn*). **f** Melonite (*me*) at pentlandite (*pn*)-silicate (*s*) grain boundary. All examples are from the semi-massive ore, except **d**, which is from a chalcopyrite veinlet

occurring as individual grains with rounded boundaries (Fig. 8a) and, rarely, with irregular and elongate shapes (Fig. 8b). The most common host-minerals are pyrrhotite, pentlandite and minor chalcopyrite. Some grains occur at the contact between sulphide and silicate.

Table 3. *Representative microprobe analyses of the different*

Ore-type	Host	Pd	Pt	Ni	Fe	Te	Bi	S	As	Total	Pd	Pt	Ni	Fe	Te	Bi	S	As	Me/nMe
		wt.%									apfu								
Merenskyite																			
SM	Po	15.31	12.50	1.35	0.91	54.00	14.27	0.08	n.d.	98.42	0.58	0.26	0.09	0.07	1.71	0.28	0.01		0.50
SM	Po	12.22	16.58	2.93	1.19	64.11	5.37	0.04	n.d.	102.44	0.43	0.32	0.19	0.08	1.88	0.10	0.005		0.51
SM	Pn	18.72	0.52	5.44	0.73	61.87	15.11	0.02	n.d.	102.41	0.63	0.01	0.33	0.05	1.73	0.26	0.002		0.51
SM	Cp	14.93	13.01	1.55	0.39	51.25	18.5	0.03	n.d.	99.66	0.57	0.27	0.11	0.03	1.65	0.36	0.004		0.49
SM	Cp	17.10	5.57	2.99	0.88	52.03	20.97	0.10	n.d.	99.64	0.63	0.11	0.20	0.06	1.59	0.39	0.01		0.50
SM	Cp	20.37	4.43	1.26	0.80	45.85	27.52	0.06	n.d.	100.29	0.77	0.09	0.09	0.06	1.45	0.53	0.01		0.51
SM	Cp-sil	11.27	14.84	4.24	1.07	65.75	5.25	0.04	n.d.	102.46	0.39	0.28	0.26	0.07	1.90	0.09	0.005		0.50
SM	Sil	21.71	0.91	2.63	0.71	57.30	17.44	0.04	n.d.	100.74	0.76	0.02	0.17	0.05	1.68	0.31	0.004		0.50
D	Cp-sil	15.52	5.15	5.01	1.56	57.34	16.94	n.d.	n.d.	101.52	0.54	0.10	0.31	0.10	1.65	0.30			0.54
Cp-vein	Cp	21.63	0.01	3.07	1.25	58.40	15.65	0.11	n.d.	100.12	0.75		0.19	0.08	1.68	0.27	0.01		0.52
Cp-vein	Cp	21.83	n.d.	2.75	0.95	57.58	16.28	0.01	n.d.	99.40	0.77		0.18	0.06	1.69	0.29	0.001		0.51
Melonite																			
SM	Po	7.66	16.75	5.68	1.37	65.41	5.18	0.07	n.d.	102.12	0.26	0.31	0.35	0.09	1.88	0.09	0.01		0.51
SM	Pn	3.46	5.17	12.94	1.53	68.42	8.45	0.37	n.d.	99.97	0.11	0.09	0.74	0.09	1.80	0.13	0.04		0.52
SM	Pn	5.25	4.77	11.48	1.44	60.99	16.05	0.11	n.d.	100.09	0.17	0.08	0.69	0.09	1.68	0.27	0.01		0.53
SM	Pn	4.32	n.d.	14.07	2.96	64.88	14.46	1.27	n.d.	101.96	0.13		0.76	0.17	1.60	0.22	0.12		0.55
Michenerite																			
SM	Po	23.2	n.d.	0.04	0.69	29.34	47.22	0.02	n.d.	100.51	0.95		0.003	0.05	1.00	0.98	0.003		0.51
SM	Sil	22.95	n.d.	0.05	0.55	28.10	46.32	0.04	n.d.	98.01	0.96		0.004	0.04	0.98	0.99	0.006		0.51
SM	Pn-sil	22.71	n.d.	0.75	1.01	29.20	47.76	0.05	n.d.	101.48	0.91		0.05	0.07	0.98	0.98	0.01		0.52
D	Po	22.79	n.d.	0.16	0.89	29.56	47.29	0.02	n.d.	100.71	0.93		0.01	0.07	1.00	0.98	0.003		0.51
Moncheite																			
SM	Pn-po	8.55	19.35	2.2	2.8	41.28	23.44	0.47	n.d.	98.09	0.34	0.41	0.16	0.21	1.35	0.47	0.06		0.60
D	Sil	2.28	35.88	0.52	1.31	53.73	5.87	0.01	n.d.	99.6	0.09	0.80	0.04	0.10	1.84	0.12	0.002		0.52
Sperrylite																			
SM	Po	0.04	56.41	0.03	0.6	0.01	0.01	0.32	42.83	100.25	0.001	0.98	0.002	0.04			0.03	1.94	0.52
SM	Pn	n.d.	57.77	0.15	0.09	0.08	0.05	0.36	40.87	99.37		1.03	0.01		0.002		0.04	1.91	0.53
SM	Sil	0.09	54.85	0.11	1.64	0.41	n.d.	0.54	40.22	97.86	0.003	0.97	0.01	0.10	0.01		0.06	1.85	0.51
D	Po	0.12	51.28	0.04	2.63	0.01	0.01	2.14	44.18	100.41	0.003	0.81	0.002	0.14			0.21	1.82	0.47

SM Semi-massive ore; *D* disseminated ore; *Cp-vein* chalcopyrite veinlets; *Po* pyrrhotite; *Pn* pentlandite; *Cp* chalcopyrite; *Sil* silicate; *n.d.* not detected; *apfu* atoms per formula unit based on a total of three atoms in the formula unit. *Me/nMe* Metal to non metal ratio. Because of the small size of the grains, there is generally interference with the adjacent minerals and traces of S and Fe are often detected, being ascribed to contamination from the host sulphides

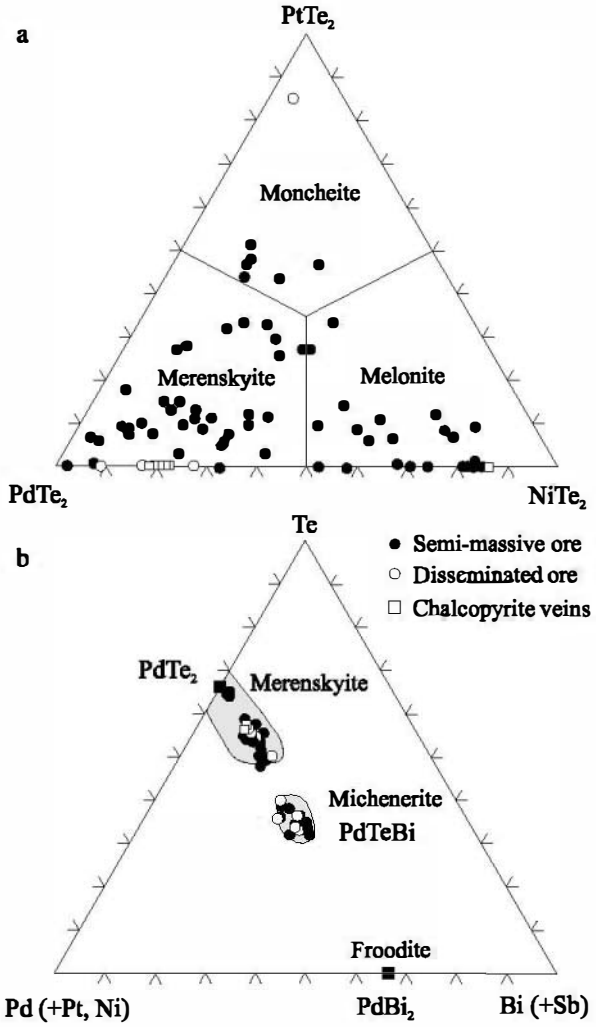

Fig. 7. **a** Modal proportions of merenskyite, melonite and moncheite from the ore-bearing breccia plotted in the $PdTe_2$-$NiTe_2$-$PtTe_2$ diagram. **b** Pd (+Pt, Ni)-Te-Bi (+Sb) diagram showing the compositional variation in at.% of merenskyite and michenerite from the ore-bearing breccia. Shaded areas represent the compositional fields of the respective minerals reported in the literature taken from *Harney* and *Merkle* (1990)

The composition of the analysed grains reveals Pd contents ranging from 32 to 36 at.%, Te from 33 to 39 at.% and Bi from 26 to 34 at.% (Fig. 7b). Pt contents are below detection limit and Ni is commonly below 1 wt.% (Table 3). Traces of Ag and Sb may substitute Pd and Bi, respectively.

Sperrylite, $PtAs_2$

Sperrylite represents 5% of the total PGM found. It occurs in the semi-massive and in the disseminated ores. Two euhedral crystals occur inside pyrrhotite with sizes of 4 μm×5 μm and 20 μm×35 μm, whereas one subhedral grain with a size of roughly 100 μm is hosted by pentlandite in contact with chlorite (Fig. 8c). This grain shows that where the faces of the sperrylite crystal are adjacent to pentlandite, they show angular blocky shapes, but, where they are in contact with chlorite, the morphology of the crystal becomes irregular (Fig. 8c). Furthermore, two small (<15 μm) crystals of sperrylite occur inside amphibole. These also exhibit corroded borders.

Sperrylite composition is almost stoichiometric with uniquely minor traces of Fe and S (<1 wt.%) (Table 3).

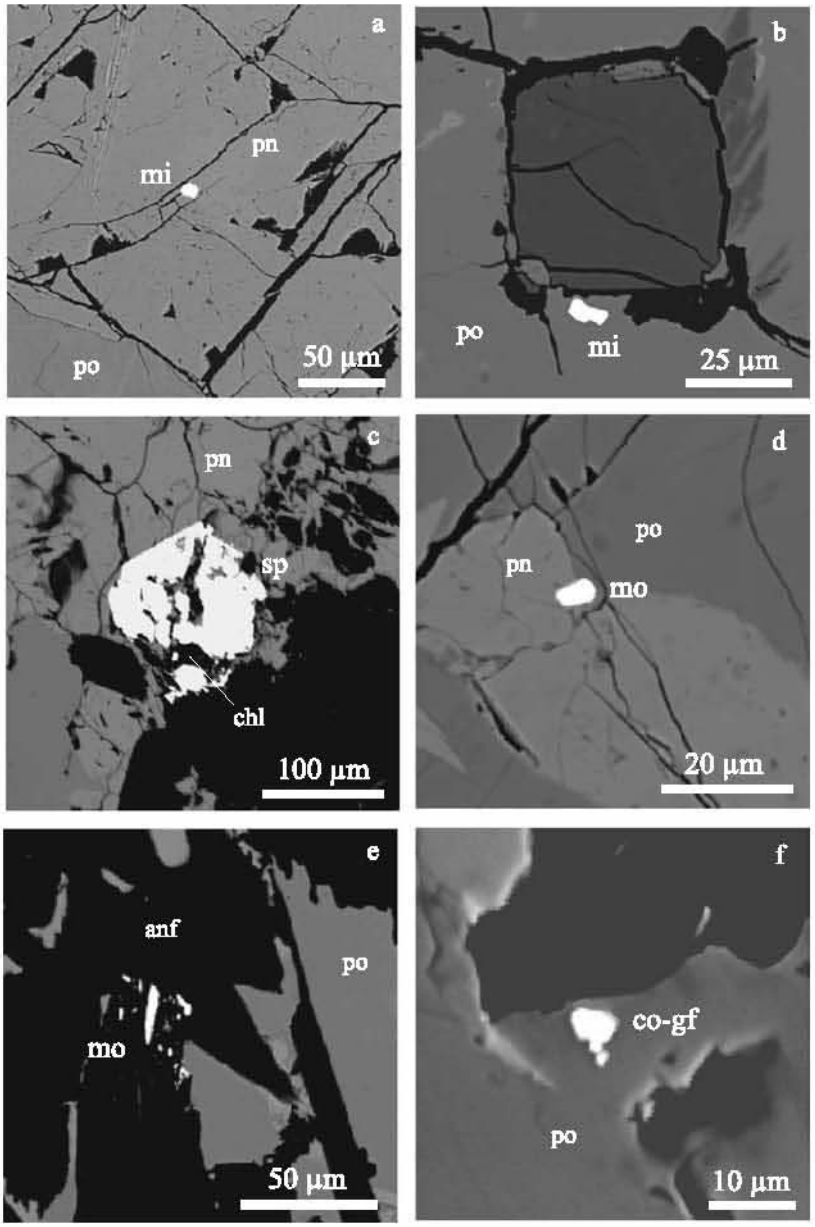

Fig. 8. Representative back-scattered electron microprobe images of the PGM. **a** Michenerite (*mi*) with rounded boundaries within pentlandite (*pn*). **b** Irregular, elongated michenerite (*mi*) grain inside pyrrhotite (*po*). **c** Single subhedral sperrylite (*sp*) crystal inside pentlandite (*pn*). Note the irregular shape of the sperrylite where it is in contact with chlorite (*chl*). **d** Subhedral moncheite (*mo*) at the interface pentlandite (*pn*)-pyrrhotite (*po*). **e** Several moncheite (*mo*) grains inside secondary amphibole (*amp*). **f** Single idiomorphic crystal of the cobaltite-gersdorffite (*co-gf*) solid solution hosted within pyrrhotite (*po*). Microphotographs **a**–**c** and **e** are from semi-massive ore, **d** and **f** from disseminated ore

Moncheite, Pt (-Pd, Ni)Te_2

Moncheite is substantially much less frequent than the other PGM described. It only represents 4% of the total PGM and occurs mostly in the semi-massive ore, as small (<10 μm), subrounded inclusions in pentlandite or in the interface pyrrhotite-pentlandite (Fig. 8d). Several irregular, elongated grains were also observed included in hydrothermal amphibole in the disseminated ore (Fig. 8e).

Its composition reveals extensive substitution of Pt for Pd (up to 10.46 wt.%) and Ni (from 1.70 to 12.12wt.%) (Fig. 7a), and of Te for Bi (from 11.39 to 25 wt.%). However, the grains located inside amphibole (Fig. 8e) exhibit a composition closer to the $PtTe_2$ end-member, containing 5.87 wt.% Bi, 2.28 wt.% Pd and 0.52 wt.% Ni.

Other PGM

The Os-Ir-As-S phases (possibly osarsite) occur enclosed in chalcopyrite from the disseminated ore, forming small rounded grains, whereas the Ir-As-S (possibly irarsite) and the Ir-Pt-As phases, always occur in a chalcopyrite veinlet.

Cobaltite-gersdorfitte, CoAsS-NiAsS

Three grains of cobaltite-gersdorffite were found in disseminated ore. They occur as single subidiomorphic crystals hosted by pyrrhotite (Fig. 8f). Their Ni, Co and Fe contents vary from 11.5 to 16.6, 13.4 to 17.9, and 3.6 to 8.3 wt.%, respectively, and they contain traces of Pd (up to 0.64 wt.%), Pt (up to 0.96 wt.%), Ir (up to 1.8 wt.%) and Rh (up to 1.7 wt.%). On the other hand, several small eu- to subhedral grains of this solid solution series were identified in a restricted area of a chalcopyrite veinlet inside chalcopyrite and pentlandite. These grains contain 22.3 wt.% Co, 8.4 wt.% Ni and 6.36 wt.% Fe, but no PGE.

Trace element contents of the Ni-Cu-Fe sulphides

Micro-PIXE analysis uniquely reveal measurable concentrations of Se (64–199 ppm), Ni (4397–48410 ppm) and Cu (95–14694 ppm) in the pyrrhotite, Se (31–201 ppm) and Zn (154 and 450 ppm) in pentlandite, Se (29–134 ppm), Ni (2383–4483ppm) and Ag (25–71ppm) in chalcopyrite and Ni (142–20666 ppm), Se (<187ppm) and As (39–534ppm) in pyrite. Pd, Ru and Rh concentrations (except in one analysis of pyrite with 22 ppm Rh) are always below their detection limits in all the analysed grains.

Discussion

Segregation and fractionation of the sulphide melt

The mineralogical assemblage composed of pyrrhotite-pentlandite-chalcopyrite occurring interstitial to a primary silicate framework, the good positive correlations between Ni, PGE and S (Fig. 3a, d), and the systematic association of PGM with magmatic sulphides support previous interpretations, which consider the Aguablanca

Ni-Cu ores as the result of the accumulation and fractional crystallisation of a magmatic sulphide melt (*Lunar* et al., 1997; *Tornos* et al., 2001; *Ortega* et al., 2004; *Piña* et al., 2006). According to these authors, the sulphide melt segregated from a fractionating silicate melt in a deep seated magma chamber and concentrated, due to its high density, in the floor of the chamber. The silicate magma together with the sulphides were later injected in the shallow crust giving rise to the orebody (e.g., Voisey's Bay deposit, *Li* and *Naldrett*, 1999). Sulphur saturation in the silicate melt could be promoted by the assimilation of S-rich black slates of the Serie Negra Formation. This is supported by sulphur and lead isotopic signatures of the ores (*Casquet* et al., 1998; *Tornos* et al., 1998), as well as by the existence of partially-digested xenoliths of black slates in the host Aguablanca gabbroic intrusion. However, S/Se ratios of the ores (from 2613 to 4710) are typical of mantle-derived sulphides (*Naldrett*, 1981) and do not support the addition of S from an external source. Nevertheless, the S/Se ratios of the Serie Negra black slates (ranging from 184 to 3300) are significantly lower than those of the ores and unusually low for this type of sedimentary rocks. Such low values can be produced by devolatilisation reactions and sulphur loss (with the consequent decrease of the S/Se ratio) associated to the transformation of pyrite to pyrrhotite in the slates (e.g., *Theriault* and *Barnes*, 1998). Thus, the mixing of these S-depleted slates with the silicate melt does not increase, but lower the S/Se ratio of the contaminated melt and, consequently, the S/Se ratio of the ores.

The different types of ores described would form by the combined effect of multiple melt injections and the fractionation of the sulphide melt. The concentric distribution of the semi-massive and the disseminated ores suggest that the disseminated ores formed earlier by the injection of a silicate melt containing dispersed droplets of unfractionated, immiscible sulphide melt. Later, a new injection of melt (containing higher proportions of immiscible sulphide melt) and carrying mafic-ultramafic fragments from the deep, partially consolidated intrusion, led to the formation of the semi-massive ores. This late injection crossed through the almost consolidated gabbronorite that hosts the disseminated ores producing the zoned structure of the Aguablanca orebody.

The semi-massive ores display mineralogical and geochemical features which suggest that they formed by the crystallisation of a monosulphide solid solution (*mss*), with partial segregation of a Cu-rich sulphide liquid. Among other things, they show: 1) large proportions of pyrrhotite and high pentlandite/chalcopyrite ratios (commonly above 4) and 2) Ni/Cu ratios significantly higher than 1 (Table 1). In contrast, the disseminated ores seem to be formed from a more fractionated sulphide melt since they show: 1) low pentlandite/chalcopyrite ratios (commonly between 0.06 and 0.31) and 2) Ni/Cu ratios commonly below unity (Table 1). However, this hypothesis is unlikely because the liquidus temperature of the silicate magma is higher than that of a fractionated sulphide liquid and thus it would be difficult for a fractionated sulphide liquid to disperse to form disseminated ore in the partially solidified igneous rocks. Therefore, the most likely hypothesis is that the disseminated ores represent an original unfractionated sulphide liquid retained as droplets in the gabbronorite.

The crystallisation of *mss* from the sulphide melt in the semi-massive ores gave rise to the segregation of a Cu-rich residual melt which mobilised away from the

core of the orebody, filling late fractures that crossed-cut the semi-massive (including some mafic-ultramafic fragments) and, mainly, the disseminated ores. These veins constitute the chalcopyrite veined ores.

Behaviour of PGE and origin of the PGM

The positive correlation between total PGE and S contents in most samples (Fig. 3d), and the close association of PGM with the base-metal sulphides are interpreted to indicate that PGE were collected by the sulphide liquid during its segregation. Thus, PGE contents of the disseminated ores would correspond to those of the parental silicate + sulphide melt, whereas PGE abundances in the semi-massive and chalcopyrite-veined ores would be the consequence of the fractional crystallisation of the sulphide melt. This interpretation is in agreement with the chemistry of the ores, since semi-massive ores are relatively richer in Os, Ir, Ru and Rh, and have lower mantle-normalised Pd/Ir ratios than the disseminated ores and the chalcopyrite-veined ores. During the crystallisation of the *mss*, this phase concentrated most Os, Ir, Ru and Rh because of their high partition coefficient between *mss* and the residual, Cu-rich sulphide melt (*Fleet* et al., 1993; *Li* et al., 1996). The remarkable correlation among these metals ($\rho > 0.97$) is a common feature of magmatic sulphide deposits (e.g., *Chai* and *Naldrett*, 1992; *Maier* and *Barnes*, 2003; *Barnes*, 2004), and evidences their similar behaviour during fractional crystallisation and their strong resistance to alteration, as it is further indicated by their mostly parallel mantle-normalised patterns (Fig. 4). Although the scarcity of Os, Ir, Ru and Rh minerals suggest that most of them should be in solid solution in pyrrhotite and pentlandite, as occurs in the Noril'sk (*Czamanske* et al., 1992; *Distler* and *Kunilov*, 1994) and Jinchuan (*Chai* et al., 1993) deposits, the obtained micro-PIXE data on Ru and Rh evidence that their concentration is always below the detection limit of the technique (4–11 ppm Ru and 6–13 ppm Rh).

During fractional crystallisation of a sulphide melt, Pt and Pd partitioned to the residual Cu-rich sulphide melt (*Fleet* et al., 1993; *Li* et al., 1996), leaving the *mss* relatively impoverished in these noble metals. Consequently, Pt and Pd should tend to concentrate in the chalcopyrite veinlets. In fact, Pd bismuthotellurides are specially abundant in these veins. However, the degree of depletion of Pt and Pd in the semi-massive ores (representing the *mss*) compared with the disseminated ores (representing the unfractionated sulphide melt) is very small (Fig. 4). This could be related with the mechanism of emplacement of the sulphide melts in shallow crustal levels. Just after each injection, thermal diffusion towards the cooler host should promote rapid cooling of the melt. This allowed to preserve the original composition of the sulphide droplets in the disseminated ores and prevented extensive fractionation of the sulphide melt in the semi-massive ores. Thus, only small amounts of Cu-rich, residual sulphide melt generated, forming some few chalcopyrite veinlets (they represent <1 vol.% of the Ni-Cu ores). In this scenario, most Pt and Pd, as well as Te, Bi and As, remained in the *mss* during the early stages of cooling and, later, exsolved giving rise to the described PGM assemblage in the semi-massive and in the disseminated ores.

Experimental results by *Hoffmann* and *MacLean* (1976) show that the Bi content of merenskyite lowers its thermal stability and that its coexistence with

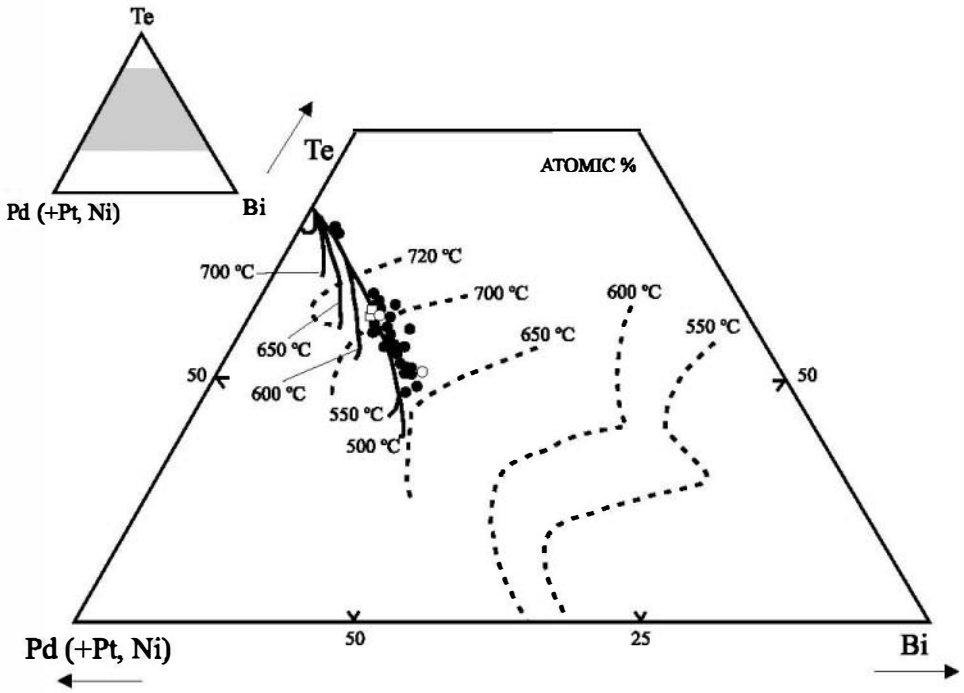

Fig. 9. Plot of merenskyites at Aguablanca in the system Pd (+Pt, Ni)-Te-Bi. Solid lines correspond to the compositions of merenskyite at different temperatures, whereas the dashed lines represent compositions of the coexisting liquid. After *Hoffman* and *MacLean* (1976). Symbols as for Figs. 3–5 and 8

michenerite limits the stability of the assemblage to temperatures below 500 °C. The merenskyite compositions at Aguablanca reveals crystallisation temperatures below 500 °C (Fig. 9). Nevertheless, more recent experiments by *Helmy* et al. (2005) (and *Helmy*, written communication) have checked the solubility of Pt, Pd and Te in a $(Fe, Cu, Ni)_{1-x}S$ melt from 1015 to 370 °C. Their results show that Pt-Pd-Ni tellurides cannot be formed at temperatures above 370 °C due to the low concentration of these elements in the original melt and their high solubility in the *mss*, which depend on the bulk Te content and the Te/(Pt + Pd) ratio of the sulphide melt. Furthermore, they show that the assemblage merenskyite-moncheite-palladian melonite can be formed only from melts with Te/(Pt + Pd) >2. As is shown in Table 2, all but one [with Te/(Pt + Pd) = 1.85] of the analysed samples from disseminated ores (representing the original, unfractionated melt) exhibit Te/(Pt + Pd) ratios above 2, in agreement with the described Pd-Pt-Ni bismuthotelluride assemblage. Consequently, the PGMs of the Aguablanca Ni-Cu deposit formed at very low temperature by exsolution from *mss* and chalcopyrite on cooling. Nevertheless, as it will be discussed below, such assemblages and the bulk distribution of some elements were partially modified by late hydrothermal fluids.

Role of hydrothermal fluids

It is well documented that Cu behaves compatibly during the segregation of a sulphide liquid from the silicate melt (*Rajamani* and *Naldrett*, 1978) and consequently

a good correlation between Cu and S would be expected. However, the lack of correlation between these elements in the Aguablanca ores suggests a redistribution of copper by secondary processes such as hydrothermal alteration (e.g., Jinchuan deposit; *Chai* and *Naldrett*, 1992).

The extensive circulation of hydrothermal fluids in Aguablanca is evidenced by the retrograde alteration of the host rocks and the replacement of pyrrhotite by pyrite in three successive episodes under progressively decreasing temperature. The precipitation of pyrite started early in the postmagmatic history of the deposit (~500 °C, Py_1) and took place along a broad period coeval with the subsolidus recrystallisation of the magmatic ores and the overall cooling of the deposit (*Ortega* et al., 2004). The hydrothermal fluids always had higher fO_2 and fS_2 than the sulphide assemblage as is indicated by the transformation of pyrrhotite into pyrite along the three recognised hydrothermal stages. However, effective copper remobilisation only took place during the second stage as shown by the occurrence of fluid-precipitated chalcopyrite along cleavage planes of secondary actinolite and chlorite, and surrounding the Py_2 crystals. The actinolite ± chlorite ± epidote ± calcite alteration assemblage indicates fluids with neutral to mild alkaline pH and circulation temperature of around 350 °C.

The high correlation between Au and Cu (Fig. 3a) indicates that gold was also mobilised by these fluids. This is further supported by its highly scattered distribution in the ores and the pronounced negative anomalies in the mantle-normalised patterns (Fig. 4).

Pt also shows negative anomalies in the different ore types (Fig. 4). Negative Pt anomalies are characteristic of sulphides representing crystallisation of *mss* (*Barnes* et al., 1997), indicating its low partition coefficient for this phase, being concentrated, like Pd, Cu and Au in the Cu-rich, residual sulphide liquid. However, in Aguablanca the occurrence of these anomalies not only in the semi-massive ore (*mss*), but also in the disseminated ores (the unfractionated original melt) and in the chalcopyrite veins (Cu-rich residual liquid) (Fig. 4) suggests that Pt also underwent hydrothermal remobilisation. Mineralogical evidence include inclusions of moncheite found in secondary actinolite (Fig. 8e) and irregular edges of sperrylite at the contact with secondary chlorite (Fig. 8c), suggesting partial dissolution of Pt-bearing phases by hydrothermal solutions.

Theoretical and experimental data (*Gammons* et al., 1992; *Wood*, 2002) show that Pd and Pt are mobile elements which can be transported in hydrothermal fluids under certain conditions. Especially, Pt is highly soluble in Cl-rich aqueous fluids at temperatures between 25 and 300 °C (*Gammons* et al., 1992). Nevertheless, if these fluids were involved in the mobilisation of Pt, as seems to be the case, negative anomalies should be observed also for Pd and this does not occur. The preferential remobilisation of Pt over Pd by postmagmatic hydrothermal fluids can be tentatively explained in terms of the factors affecting the solubility of these metals in the aqueous fluid.

In magmatic-hydrothermal environments, between 500 and 300 °C, copper is preferentially dissolved in hypersaline, neutral-weak acidic, and intermediate-reduced solutions and mainly transported as $CuCl_2^-$ (*Liu* and *McPhail*, 2005 and references therein). Major factors controlling chalcopyrite deposition are decrease of temperature, and salinity (i.e., Cl availability), and to a lesser extend, decrease of

fO_2 and increase of pH and fS_2. At Aguablanca, where geochemical and mineralogical evidences indicate that chalcopyrite was remobilised by hydrothermal fluids and precipitated again at around 350 °C, these factors would have competed among them in the solubility reactions of copper and therefore, dissolution of chalcopyrite was limited. As the fluids circulated and the deposit cooled down, the fluid became saturated in chalcopyrite around 350 °C and the decrease of temperature probably played a major role.

Gold can be transported either as $Au(HS)_2^-$ or as $AuCl_2^-$, the latter being the dominant complex above 300 °C (*Romberger*, 1991). The stability of the $AuCl_2^-$ strongly decreases with decreasing temperature and salinity. This is, therefore in agreement with the mobilisation, transport, and precipitation of copper indicated above.

Pt and Pd can also be transported as chloride complexes at temperatures above 300 °C, $PtCl_3^-$ and $PdCl_4^{2-}$, respectively, being the dominant species (*Wood*, 2002). At given pH, a[Cl^-], and fO_2 conditions, these metals exhibit retrograde solubility, i.e., their solubility decrease as temperature increases. However, if the fO_2 is buffered by a mineralogical assemblage, as it is in Aguablanca by the transformation pyrrhotite → pyrite in the postmagmatic stages, the solubility decreases with decreasing temperature. In addition, as any chloride complex, the Pd and Pt-complexes stabilities are strongly dependent of the salinity (i.e., a [Cl^-]). This is a key point in understanding the different behaviour of Pt against Pd during the hydrothermal remobilisation of metals. At temperatures above 300 °C, Cu, Au, Pt and Pd will be transported in solution as $CuCl_2^-$, $AuCl_2^-$, $PtCl_3^-$ and $PdCl_4^{2-}$, respectively. Thus, in a fluid with a given concentration of chlorine, the facility of forming chloride complexes increases following the order Pd → Pt → Cu, Au. Therefore, the avidity of copper for chlorine, together with the much higher abundance of copper than Pt and Pd in the deposit, will result in a preferential dissolution of copper, and subsequently of gold, over Pt and Pd. This could drastically reduce the availability of chlorine to form Pt and Pd complexes, thus resulting in a very limited remobilisation of Pt (most of the Pt minerals remain in the sulphide ore) and a negligible dissolution of Pd, more sensitive to the a[Cl^-]) of the fluid than Pt. The metal remobilisation, developed at T> 350 °C probably was partially coeval with the exsolution of Pd and Pt from the *mss* below 370 °C, and this could aid to the observed Pt remobilisation.

Acknowledgements

The authors are very grateful to Río Narcea Recursos S. A. (owner of the deposit) and especially to Mr. C. Maldonado and C. Martínez for the facilities given for carrying on of this research. We greatly acknowledge Prof. H. Helmy for his help in the discussion of the genesis of Pt-Pd-Ni bismuthotellurides, allowing us to use his partly unpublished experimental data. Our work has greatly benefited from the discussions with Prof. S. Wood at the 10th Platinum Symposium at Oulu. Professor J. González de Tánago and Mr. A. Larios kindly assisted in the electron-probe micro-analyses. We thank Prof. J. L. Campbell of the Guelph University for his assistance during the PIXE analyses. We thank two reviewers, Prof. S. J. Barnes and C. Ferreira, for their constructive reviews and Tuomo Alapieti for his editorial input which have helped to improve the manuscript. This research was supported by the Spanish Ministry of Education and Science, Project BTE2003-03599.

References

Barnes SJ (2004) Komatiites and nickel sulphides ores of the Black Swan area, Yilgarn Craton, Western Australia. 4. Platinum group element distribution in the ores, and genetic implications. Mineral Deposita 39: 752–765

Barnes SJ, Lightfoot PC (2005) Formation of magmatic nickel-sulfide ore deposits and processes affecting their copper and platinum-group elements contents. In: *Hedenquist JW, Thompson JFH, Goldfarb RJ, Richards JP* (eds) Economic Geology One Hundreth Anniversary Volume, pp 179–213

Barnes SJ, Makovicky E, Makovicky M, Rose-Hansen J, Karup-Moller S (1997) Partition coefficients for Ni, Cu, Pd, Pt, Rh and Ir between monosulphide solid solution and sulfide liquid and the formation of compositionally zoned Ni-Cu sulfide bodies by fractional crystallization of sulfide liquid. Can J Earth Sci 34: 366–374

Barnes SJ, Boyd R, Korneliussen A, Nilsson LP, Often M, Pedersen RB, Robins B (1988) The use of mantle normalization and metal ratios in discriminating between the effects of partial melting, crystal fractionation and sulphide segregation on platinum-group elements, gold, nickel and copper: examples from Norway: In: *Prichard HM, Potts PJ, Bowles JFW, Cribb SJ* (eds) Geo-platinum 87. Elsevier, London, pp 113–143

Cabri LJ (2002) The platinum-group minerals: In: *Cabri LJ* (ed) The geology, mineralogy and mineral beneficiation of platinum-group elements. Canadian Institute of Mining and Metallurgy, Spec Vol. 54, pp 13–129

Casquet C, Eguiluz L, Galindo C, Tornos F, Velasco F (1998) The Aguablanca Cu-Ni-(PGE) intraplutonic ore deposit (Extremadura, Spain). Isotope (Sr, Nd, S) constraints on the source and evolution of magmas and sulphides. Geogaceta 24: 71–72

Casquet C, Galindo C, Tornos F, Velasco F, Canales A (2001) The Aguablanca Ni-Cu-(PGE) intraplutonic ore deposit (Extremadura, Spain), a case of synorogenic orthomagmatic mineralization: age and isotope composition of magmas (Sr, Nd) and (S). Ore Geol Rev 18: 237–250

Chai G, Naldrett AJ (1992) PGE mineralization of the Jinchuan Ni-Cu sulfide deposit, NW China. Econ Geol 87: 1475–1495

Chai G, Naldrett AJ, Rucklidge JC, Kilius LR (1993) In situ quantitative analyses of PGE and Au in sulfide minerals of the Jinchuan Ni-Cu deposit by accelerator mass spectrometry. Can Mineral 31: 19–30

Czamanske GK, Kunilov VR, Zientek ML, Cabri LJ, Likhachev AP, Calk LC, Oscarson RL (1992) A proton-microprobe study of magmatic sulfide ores from the Noril'sk-Talnakh district, Siberia. Can Mineral 30: 249–287

Daltry VV, Wilson VE (1997) Review of platinum-group mineralogy: compositions and elemental associations of the PG-minerals and unidentified PGE-phases. Mineral Petrol 60: 185–229

Distler VV, Kunilov VE (1994) Geology and ore deposit of the Noril'sk region. Guidebook, VII International Platinum Symposium. The International Association on the genesis of ore deposits. Russian academy of science, Moscow, 67 pp

Eguiluz L, Gil Ibarguchi JI, Abalos B, Apraiz A (2000) Superposed Variscan and Cadomian orogenic cycles in the Ossa-Morena zone and related areas of the Iberian Massif. Geol Soc Am Bull 112: 1398–1413

Evans-Lamswood DM, Butt DP, Jackson RS, Lee DV, Muggridge MG, Wheeler RI, Wilton DHC (2000) Physical controls associated with the distribution of sulfides in the Voisey's Bay Ni-Cu-Co deposit, Labrador. Econ Geol 95: 749–769

Fleet ME, Chryssoulis SL, Stone WE, Weisener CG (1993) Partitioning of platinum-group elements and Au in the Fe-Ni-Cu-S system: experiments on the fractional crystallization of sulphide melt. Contrib Mineral Petrol 115: 36–44

Gammons CH, Bloom MS, Yu Y (1992) Experimental investigations of the hydrothermal geochemistry of platinum and palladium. I. Solubility of platinum and palladium sulphide minerals in $NaCl/H_2SO_4$ solutions at 300 °C. Geochim Cosmochim Acta 56: 3881–3894

Gervilla F, Kojonen K (2002) The platinum-group minerals in the upper section of the Keivitsansarvi Ni-Cu-PGE deposit, northern Finland. Can Mineral 40: 377–394

Harney DMW, Merkle RKW (1990) Pt-Pd minerals from the upper zone of the Bushveld Complex, South Africa. Can Mineral 28: 619–628

Helmy HM, Ballhaus C, Berndt-Gerdes J (2005) The formation of Pt, Pd and Ni tellurides during cooling of Fe-Ni-Cu sulphide: results of experiments and implications for natural systems. Geochem Miner Petrol 43: 87–92

Hoffman E, MacLean WH (1976) Phase relations of michenerite and merenskyite in the Pd-Bi-Te system. Econ Geol 71: 1461–1468

Li C, Naldrett AJ (1999) Geology and petrology of the Voisey's Bay intrusion: reaction of olivine with sulfide and silicate liquids. Lithos 47: 1–31

Li C, Barnes SJ, Makovicky E, Rose-Hansen J, Makovicky M (1996) Partitioning of Ni, Cu, Ir, Rh, Pt and Pd between monosulphide solid solution and sulphide liquid: effects of composition and temperature. Geochim Cosmochim Acta 60: 1231–1238

Liu W, McPhail DC (2005) Thermodynamic properties of copper chloride complexes and copper transport in magmatic-hydrothermal solutions. Chem Geol 221: 21–39

Lunar R, García-Palomero F, Ortega L, Sierra J, Moreno T, Prichard H (1997) Ni-Cu-(PGM) mineralization associated with mafic and ultramafic rocks: the recently discovered Aguablanca ore deposit, SW Spain. In: *Papunen H* (ed) Mineral deposits: research and exploration. Where do they meet? Balkema, Rótterdam, pp 463–466

Maier WD, Barnes SJ (2003) Platinum group elements in the Boulder Belt, western Bushveld complex, South Africa. Mineral Deposita 38: 370–380

Maxwell JA, Campbell JL, Teesdale WJ (1989) The Guelph PIXE software package. Nucl Instr Methods Phys Res 43: 218–230

McDonough WF, Sun SS (1995) The composition of the Earth. Chem Geol 120: 223–253

Naldrett AJ (1981) Nickel sulfide deposits: classification, composition and genesis. Econ Geol 75: 628–685

Ortega L, Moreno T, Lunar R, Prichard H, Sierra J, Bomati O, Fisher PC, García Palomero F (1999) Minerales del grupo del platino y fases asociadas en el depósito de Ni-Cu-EGP de Aguablanca, SW España. Geogaceta 25: 155–158

Ortega L, Prichard H, Lunar R, García Palomero F, Moreno T, Fisher PC (2000) The Aguablanca discovery. Mineral Mag 2: 78–80

Ortega L, Lunar R, García Palomero F, Moreno T, Prichard H (2001) Remobilización de minerales del grupo del platino en el yacimiento de Ni-Cu-EGP de Aguablanca (Badajoz). Boletín de la Sociedad Española de Mineralogía 24: 175–176

Ortega L, Lunar R, García Palomero F, Moreno T, Martín Estévez JR, Prichard HM, Fisher PC (2004) The Aguablanca Ni-Cu-PGE deposit, southwestern Iberia: magmatic ore-forming processes and retrograde evolution. Can Mineral 42: 325–350

Piña R, Lunar L, Ortega L, Gervilla F, Alapieti T, Martínez C (2004) Origen de los fragmentos máficos-ultramáficos de la brecha mineralizada del yacimiento de Ni-Cu-EGP de Aguablanca (Badajoz). Revista de la Sociedad Española de Mineralogía 2: 19–20

Piña R, Gervilla F, Ortega L, Lunar R (2005) Geochemistry and mineralogy of platinum-group elements in the Aguablanca Ni-Cu deposit (SW Spain). In: *Törmänen TO, Alapieti TT* (eds) Platinum-group elements – from genesis to beneficiation and environmental impact, 10th Int. Platinum Symposium, Extended Abstracts, Oulu, pp 215–218

Piña R, Lunar L, Ortega L, Gervilla F, Alapieti T, Martínez C (2006) Crystal fractionation and sulfide segregation processes in the source chamber of the Aguablanca Ni-Cu-PGE deposit (SW Spain). Econ Geol (in press)

Quesada C (1991) Geological constraints on the Paleozoic tectonic evolution of the tectonostratigraphic terranes in the Iberian Massif. Tectonophysics 185: 225–245

Quesada C, Munha J (1990) Metamorphism. In: *Dallmeyer RD, Martínez García E* (eds) Premesozoic Geology of Iberia. Springer Verlag, Heidelberg, pp 314–320

Quesada C, Fonseca PE, Munhá PE, Oliveira JM, Ribeiro A (1994) The Beja-Acebuches Ophiolite (Southern Iberia Variscan foldbelt): geological characterization and geodynamic significance. Boletín Geológico y Minero 105: 3–49

Rajamani V, Naldrett AJ (1978) Partitioning of Fe, Co, Ni and Cu between sulphide liquid and basaltic melt and the composition of Ni-Cu sulfide deposits. Econ Geol 73: 82–93

Riveiro A, Quesada C, Dallmeyer RD (1990) Geodynamic evolution of the Iberian Massif. In: *Dallmeyer RD, Martínez García E* (eds) Premesozoic geology of Iberia. Springer Verlag, Heidelberg, pp 399–409

Romberger SB (1991) Transport and deposition of precious metals in epithermal deposits. In: *Raines GL, Lisle RE, Richard E, Schafer RW, Wilkinson WH* (eds) Geology and ore deposits of the Great Basin. Symposium Proc. Geol Soc Nevada, Reno, Nevada, pp 219–232

Romeo I, Lunar R, Capote R, Quesada C, Dunning GR, Piña R, Ortega L (2004) Edades de cristalización U-Pb en circones del complejo ígneo de Santa Olalla de Cala: implicaciones en la edad del yacimiento de Ni-Cu-EGP de Aguablanca (Badajoz). Revista de la Sociedad Española de Mineralogía 2: 29–30

Sánchez Carretero R, Eguiluz L, Pascual E, Carracedo M (1990) Igneous rocks of the Ossa-Morena Zone. In: *Dallmeyer RD, Martínez García E* (eds) Premesozoic geology of Iberia. Springer Verlag, Heidelberg, pp 292–313

Theriault RD, Barnes SJ (1998) Compositional variations in Cu-Ni-PGE sulphides of the Dunka road deposit, Duluth complex, Minnesota: the importance of combined assimilation and magmatic processes. Can Mineral 36: 869–886

Tornos F, Chiaradia M, Fontboté L (1998) La geoquímica isotópica del plomo en las mineralizaciones de la Zona de Ossa Morena (ZOM): implicaciones metalogenéticas y geotectónicas. Boletín de la Sociedad Española de Mineralogía 21: 206–207

Tornos F, Casquet C, Galindo C, Velasco F, Canales A (2001) A new style of Ni-Cu mineralization related to magmatic breccia pipes in a transpressional magmatic arc, Aguablanca, Spain. Mineral Deposita 36: 700–706

Tornos F, Iriondo C, Casquet C, Galindo C (2004) Geocronología Ar–Ar de flogopitas del stock de Aguablanca (Badajoz). Implicaciones sobre la edad del plutón y de la mineralización de Ni-(Cu) asociada. Geotemas 6: 189–192

Wood SA (2002) The aqueous geochemistry of the platinum-group elements with applications to ore deposits. In: *Cabri LJ* (ed) The geology, mineralogy and mineral beneficiation of platinum-group elements. Canadian Institute of Mining and Metallurgy, Spec Vol. 54, pp 211–249

Authors' addresses: *R. Piña* (corresponding author; e-mail: rpinagar@geo.ucm.es), *L. Ortega* (e-mail: lortega@geo.ucm.es), *R. Lunar* (e-mail: lunar@geo.ucm.es), Departamento de Cristalografía y Mineralogía, Facultad de Geología, Universidad Complutense de Madrid, ES-28040 Madrid, Spain; *F. Gervilla* (e-mail: gervilla@ugr.es), Facultad de Ciencias, Instituto Andaluz de Ciencias de la Tierra, Universidad de Granada-CSIC, Avda. Fuentenueva, s/n, ES-18002 Granada, Spain